Energy, Exergy and Sensitivity Analysis of a Novel Multi-Generation Solar-Based System: Integrating Concentrated Solar Power, Modified Kalina Cycle, and Heat Pump

Energy, exergy and sensitivity analysis of a novel multi-generation solar-based system: integrating concentrated solar power, modified Kalina cycle, and heat pump

Ali Shokri Kalan[a,*], Mohammadreza Babaei Khuyinrud[b], Xiaoshu Lü[a],

[a] Renewable Energy and Built Environment, University of Vaasa, P.O. Box 700, FIN-65101 Vaasa, Finland

[b] Faculty of Mechanical Engineering, Sahand University of Technology, P.O. Box 51335-1996, Sahand New Town, Tabriz, Iran

***Corresponding author: Ali.Shokrikalan@uwasa.fi (Ali Shokri Kalan)**

Abstract

Amid rising global energy demand and environmental concerns, the development of sustainable, efficient energy systems is critical. This study introduces a novel solar-driven integrated system designed for the simultaneous generation of power, heating, and cooling. The system incorporates three main subsystems: a concentrated solar power unit with thermal energy storage, a modified Kalina cycle utilizing an ammonia–water mixture, and a heat pump operating with toluene. Thermodynamic analysis yields overall energy and exergy efficiencies of 25.6% and 6.8%, respectively, with outputs of 3,300 kW power, 2,500 kW cooling, and 14,300 kW heating. Exergy destruction analysis reveals that the concentrated solar power subsystem is the largest contributor to irreversibility, accounting for 69.02% of total exergy destruction, followed by the Kalina cycle (19.2%) and the heat pump (11.8%). The heliostat field and receiver within the concentrated solar power subsystem are the most critical components, responsible for 40.6% and 28.4% of total exergy losses, respectively. A sensitivity analysis was conducted on four key parameters. Results indicate that increasing direct normal irradiance and turbine inlet temperature reduces energy efficiency but enhances exergy efficiency due to greater work output. Higher turbine isentropic efficiency improves both efficiencies, while a higher compressor pressure ratio has minimal impact on energy efficiency and slightly lowers exergy efficiency. These findings emphasize the importance of optimizing operating conditions to improve overall system performance.

Keywords:

Renewable energy, concentrated solar power system, modified Kalina cycle, sensitivity analysis, energy and exergy analysis, net zero emissions

1. Introduction

The global dependence on fossil fuels has led to critical issues such as climate change, environmental degradation, and the depletion of finite resources [1]. To tackle these challenges, extensive research has focused on promoting renewable energy sources (RES) — including solar, wind, geothermal, wave energy, and biomass — as sustainable alternatives to conventional fossil-based energy systems [2]. Solar energy is globally acknowledged as a plentiful, clean, sustainable, and economically viable form of renewable energy. Countries around the world have embraced innovative technologies to harness and expand the use of solar power [3].

Advanced energy conversion systems like ORC, Brayton, supercritical CO_2, and Kalina cycles—individually or in hybrid forms—enhance the efficiency of renewable energy use. Cogeneration systems, such as CCHP and other multi-generation configurations, further improve overall performance by integrating complementary subsystems. Their strategic deployment supports energy demand and contributes to carbon neutrality. Solar energy can be harnessed through two primary technologies: photovoltaic (PV) systems and concentrated solar power (CSP) systems. CSP utilizes direct solar radiation by focusing sunlight with mirrors or lenses to heat a working fluid, thereby enabling thermal energy conversion and storage [4]. Among renewable energy technologies, concentrated solar power (CSP) stands out as a highly promising and cost-effective option for generating clean, reliable, and efficient electricity [5]. Danish et al. studied a particle-based CSP system integrated with an exhaust gas absorption chiller in Tabuk, Saudi Arabia, delivering 191 TWh of electricity and 97.5 million TR-h of cooling annually (COP 1.46). The levelized costs—¢6.1 /kWh for electricity and ¢3.8 /TR-h for cooling—were lower than those of conventional systems [6].

Alharthi et al. developed a CO_2-based solar-powered system for combined power, heat, and cooling, achieving up to 72% efficiency. The solar collector had the highest irreversibility, and results aligned well with theoretical predictions [7].Parvez et al. analyzed a solar-driven trigeneration system in the Middle East, achieving over 60% energy efficiency and notable emission reductions. The system saved $4.45 million annually with a 6.66-year payback period, highlighting strong economic and environmental benefits [8]. A major challenge in renewable energy utilization is managing intermittency to ensure sustainability and reliability. Energy storage solutions—such as TES, CAES, batteries, and hydrogen—help address this issue, with thermal energy storage playing a key role in stabilizing heating and cooling applications [9]. Boukelia et al. assessed four CSP systems enhanced with TES, fuel backup, waste heat recovery, and a Kalina cycle. PT Oil achieved the highest power (235 GWh) and WHR (37 GWh), ST DSG had the highest WHR efficiency (14.7%), while PT MS offered the best economics with $15.2/MWh cost and $257.4M NPV [10]. Singh et al. studied a solar-powered PEM hydrogen system using a parabolic trough collector, TES, and a Kalina cycle. TES supplied up to 377 kW of heat, enabling

58.8 kW net power and 0.75 kg/day hydrogen production at $9.16/kg, demonstrating efficient energy and hydrogen integration [11].

Based on the literature, numerous studies have explored renewable-based energy systems. While many focus on concentrated solar power (CSP) for its feasibility and cost-effectiveness, sustainability aspects are often under-addressed. Thermal energy storage (TES) is recognized as a mature and reliable solution, yet its integration with CSP systems remains insufficiently studied. Moreover, the potential of combined cooling, heating, and power (CCHP) or multi-generation systems—particularly those with optimized subsystems—for improving overall efficiency is frequently overlooked. This study proposes a novel and efficient CCHP system integrating CSP, a modified Kalina cycle, and a heat pump. TES is utilized in the CSP section to address solar intermittency. The modified Kalina cycle, using an ammonia–water working fluid, simultaneously generates power and cooling, with a specialized distillation column (rectifier, partial condenser, and reboiler) enhancing refrigerant separation and cooling capacity. A heat pump is also integrated to recover waste heat and meet heating demand. The main contributions of this study are as follows:- Development of a clean trigeneration energy system powered by solar energy.

- Proposal of a modified Kalina subsystem for power generation and enhanced cooling capacity, utilizing a novel distillation column for optimal ammonia separation.

- Integration of thermal energy storage (TES) to improve system reliability, and utilization of waste heat to operate a heat pump for heating production.

- Implementation of comprehensive energy and exergy analyses to evaluate system performance and efficiency.

- Execution of sensitivity analysis to identify key parameters affecting system efficiency and overall performance.

2. System description

As shown in Figure 1, the proposed novel and efficient renewable-based energy system is composed of three integrated subsystems, collectively capable of producing power, cooling, and heating. These subsystems are: a concentrated solar power (CSP) system, a modified Kalina cycle, and a heat pump.

The CSP subsystem comprises a heliostat field, solar tower, pump, and hot and cold thermal storage units to ensure continuous operation. Molten salt (state 42) is pressurized by pump 4 (P4) and then heated in the receiver (state 38). The heated molten salt (state 39) transfers its thermal energy first to the boiler (state 40) and then to the reboiler (state 41) to drive the modified Kalina cycle. Afterwards, it enters a heat exchanger (HEX) to provide the necessary heat for operating the heat pump subsystem.

The working fluid in the modified Kalina cycle is an ammonia–water mixture. Initially, the fluid (state 10) enters the boiler, where it is heated and then directed as high-temperature vapor (state

13) to the turbine for expansion and power generation. The turbine exhaust (state 14) flows through Recuperator 1 (Rec1), where it transfers heat to cooler streams, before mixing with three other streams (state 15) and entering Absorber 1 (Abs1) to release heat (state 16). The outlet stream from Abs1 (state 1) is pressurized by Pump 1 (P1) to a higher pressure (state 2) and then split into two branches. The first branch (state 2′) passes through Rec1 as a cold stream, is further preheated in Recuperator 2 (Rec2) (state 3′), and enters the separator (Sep) as stream 4. Inside the separator, it is divided into two saturated streams: a liquid stream (4′) and a vapor stream (4″). The liquid stream (4′) releases heat in Preheater 1 (Pre1), flows through Valve 2 (state 5), and joins other streams in the Mixer (Mix) (state 6). The vapor stream (4″) passes through Preheater 2 (Pre2) as stream 7. The second branch from state 2 (state 2″) mixes with stream 7 and enters Absorber 2 (Abs2), where heat is released (state 7′). The outlet stream (state 8) is again divided into two paths. One path (state 8′) is pressurized by Pump 2 (P2), passes through Pre1, and returns to the boiler. The other path (state 8″) is pressurized by Pump 3 (P3), heated in Pre2 (state 17), and enters the rectifier (state 18). In the rectifier, ammonia-rich vapor rises to the partial condenser (P.Con), producing a high-concentration ammonia solution. This stream exits as state 19, flows through the condenser (Con), and enters the subcooler (state 20). After releasing heat, it is depressurized via Valve 5 and used to provide cooling in the evaporator (state 22). The outlet stream (state 23) gains heat before entering the Mix (state 24). Simultaneously, the ammonia-lean solution exits the bottom of the reboiler (state 25), preheats a cold stream (state 26), is depressurized via Valve 4, and enters the Mix (state 27).

In the heat pump subsystem, toluene is used as the working fluid. It first enters the heat exchanger (HEX) at state 46 to absorb heat, and then flows into the compressor (Comp) at state 43. After compression, the fluid exits at high pressure and high temperature (still state 43) and is utilized as a heat source in the heater to meet the system's thermal demand. The outlet stream from the heater (state 45) then passes through Valve 6 (V.6), where its pressure is reduced, and the fluid re-enters the cycle, returning to the HEX.

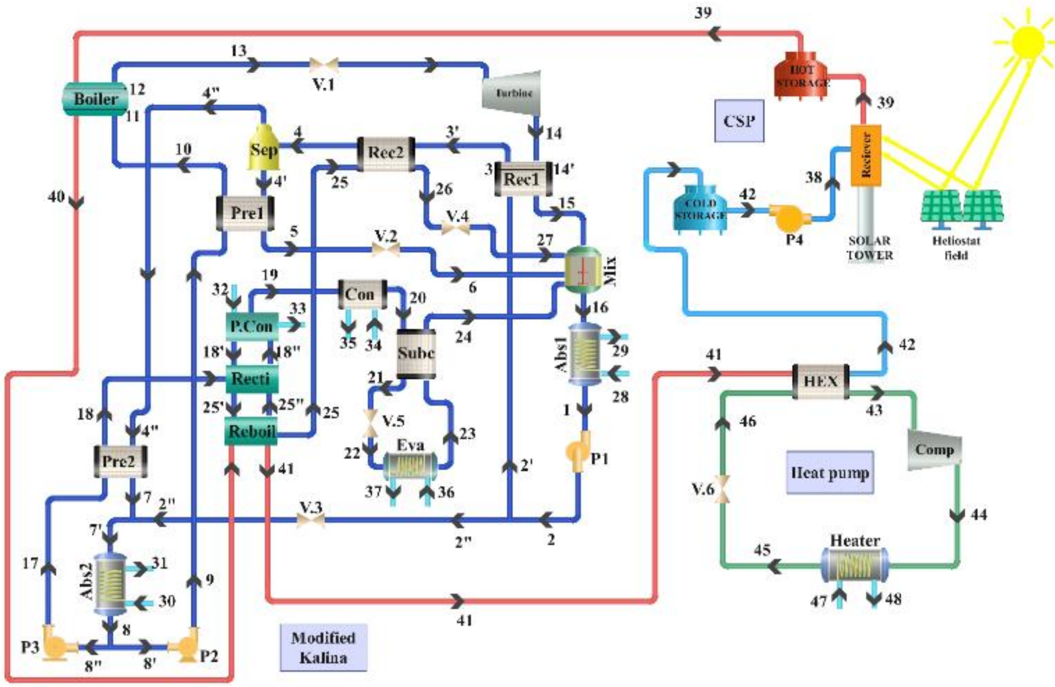

Figure. 1. Schematic of the proposed system

3. Methodology

The reference temperature and pressure are 298.15 K and 1 bar, respectively [12]. All of the necessary input data for modelling are reported in Table 1.

Table1. Input data for thermodycnamic modeling

subsystem	**Inputs**			
	Components	***Value***	***unit***	***Ref***
Concentrated Solar Power	DNI	850	(W/m^2)	[13]
	η_{cos}	0.8267	-	
	$\eta_{s\&b}$	0.9698	-	
	η_{int}	0.9710	-	
	η_{att}	0.9383	-	
	η_{ref}	0.88	-	
	N_{hel}	760	-	
	A_{hel}	9.45*12.84	(m^2)	
	A_{rec}	68.1	(m^2)	
Modified Kalina	$\eta_{Turbine}$	0.87	-	[14]
	η_{pump}	0.75	-	

subsystem	Inputs			
	Components	***Value***	***unit***	***Ref***
	x_{19}	0.998	-	
	Quality, Q_{23}	95	%	
	$\Delta T_{Heat\ exchagers}$	5	K	
	x_1	0.3408	-	
	T_{13}	653.1	K	
	T_{36}	260.15	K	
Heat Pump	$\eta_{Compressor}$	0.85	-	[15]
	T_{43}	330	K	
	Quality, Q_{43}	100	%	
	$PR_{Compressor}$	3.7	-	
	ΔT_{Heater}	5	K	

The first step involves a thermodynamic analysis of the system, with the corresponding relations outlined below [16]:

$$\dot{Q} - \dot{W} + \sum_i \dot{m}_\iota \left(h_i + \frac{V_i^2}{2} + g z_i \right) - \sum_e \dot{m}_e \left(h_e + \frac{V_e^2}{2} + g z_e \right) = \frac{dE}{dt} \tag{1}$$

$$\sum_i \dot{m}_\iota = \sum_e \dot{m}_e \tag{2}$$

Due to the binary solution used in the Kalina subsystem, the concentration balance is outlined as follows:

$$\sum_i \dot{m}_\iota x_i = \sum_e \dot{m}_e\, x_e \tag{3}$$

Where x denotes the mass ratio of ammonia in the solution. In the CSP subsystem the useful heat absorbed by the receiver and optical efficiency of the heliostat field, η_{field} can be calculated as [17]:

$$\dot{Q}_{rec,in} = \eta_{field} . (DNI). A_{hel} . N_{hel} \tag{4}$$

$$\eta_{field} = \eta_{fcos} . \eta_{s\&b} . \eta_{int} . \eta_{att} \eta_{ref} \tag{5}$$

where η_{fcos}denotes the cosine effect efficiency; $\eta_{s\&b}$represents the shading and blocking efficiency; η_{int} represents the interception efficiency; $\eta_{att}$is the atmospheric attenuation efficiency and η_{ref} represents the reflectivity of the heliostats. Additionally, assuming negligible changes in potential and kinetic exergy, the physical and chemical exergy can be calculated using the following equation:

$$\dot{E}_{ph} = \dot{m}(h - h_0) - T_0(s - s_0) \quad (6)$$

$$\dot{E}_{ch} = \frac{\dot{m}_k}{M_k}\bar{e}_k^{ch} \quad (7)$$

Where M_k is the molecular weight of species k, and $\bar{e}_k^{ch}$ is the chemical exergy per mole of species k. The chemical exergy for ammonia-water solution can be calculated using the following equation [18]:

$$\dot{E}_{ch,solution} = \dot{m}\left[\left(\frac{x_{NH3}}{M_{NH3}}\right)e^0_{ch,NH3} + \left(\frac{1 - x_{NH3}}{M_{H2O}}\right)e^0_{H2O}\right] \quad (8)$$

Total exergy for a stream can be defined as follows:

$$\dot{E} = \dot{E}_{ph} + \dot{E}_{ch} \quad (9)$$

The exergy balance for each control volume is used to calculate component-wise exergy destruction.

$$\dot{E}_{D,k} + \dot{E}_{Loss,k} = \dot{E}_{F,k} - \dot{E}_{P,k} \quad (10)$$

In which, the subscripts ″D″, ″F″, and ″P″ indicate destruction, fuel, and product exergy, respectively. Furthermore, the first and second law efficiencies of the proposed cogeneration system are evaluated using the following expressions:

$$\eta_I = \frac{\dot{W}_{net} + \dot{Q}_{Heater} + \dot{Q}_{Eva,Kalina}}{\dot{Q}_{Sun}} \quad (11)$$

$$\eta_{II} = \frac{\dot{W}_{NET} + \dot{Q}_{Cooling}\left(\frac{T_0}{T_{ref.cold}} - 1\right) + \dot{Q}_{Heating}\left(1 - \frac{T_0}{T_{ref.hot}}\right)}{\dot{Q}_{Sun}\left(1 - \frac{T_0}{T_{sun}}\right)} \quad (12)$$

4. Results and Discussion

4.1. Validation

Table 2 and Table 3 show the energy and exergy balance equations and the validation results for each system compared with reference studies, respectively, demonstrating good agreement.

Table 2. Energy and exergy balance equations for the components of the proposed system

Components	Balance equations		Components	Balance equations	
	Energy	*Exergy*		*Energy*	*Exergy*
Heliostat field	$\dot{Q}_{rec,in} = \eta_{field}.(DNI).A_{hel}.N_{hel}$	$\dot{E}_{D,helio} = \dot{Q}_{sun}\left(1-\frac{T_0}{T_{sun}}\right) - \dot{Q}_{rec,in}(1-\frac{T_0}{T_{hel}})$	*Throttle valve 2*	$\dot{m}_5 h_5 = \dot{m}_6 h_6$	$\dot{E}_{D,Tv2} = \dot{E}_5 - \dot{E}_6$
Receiver	$\eta_{rec} = \frac{\dot{Q}_{rec,net}}{\dot{Q}_{rec,in}}$, $\dot{Q}_{rec,in} = \dot{Q}_{rec,net} + \dot{Q}_{rec,loss}$ $\dot{Q}_{rec,net} = \dot{m}_{39}(h_{39}-h_{38}) + \dot{Q}_{rec,loss}$	$\dot{E}_{D,rec} = \dot{E}_{38} + \dot{Q}_{rec.in}\left(1-\frac{T_0}{T_{ref,hel}}\right) - \dot{E}_{39} - \dot{Q}_{rec,loss}$	*Throttle valve 4*	$\dot{m}_{26}h_{26} = \dot{m}_{27}h_{27}$	$\dot{E}_{D,Tv4} = \dot{E}_{26} - \dot{E}_{27}$
CSP pump	$\dot{W}_{pump,CSP} = \dot{m}_{38}(h_{38}-h_{42})$	$\dot{E}_{D,pum} = \dot{W}_{pump,CSP} - (\dot{E}_{38} - \dot{E}_{42})$	*Throttle valve 5*	$\dot{m}_{21}h_{21} = \dot{m}_{22}h_{22}$	$\dot{E}_{D,Tv5} = \dot{E}_{21} - \dot{E}_{22}$
Boiler	$\dot{Q}_{Boil} = \dot{m}_{10}(h_{13}-h_{10}) = \dot{m}_{39}(h_{39}-h_{40})$	$\dot{E}_{D,Boil} = \dot{E}_{10} + \dot{E}_{39} - \dot{E}_{13} - \dot{E}_{40}$	*Subcooler*	$\dot{Q}_{Sub} = \dot{m}_{20}(h_{20}-h_{21}) = \dot{m}_{24}(h_{24}-h_{23})$	$\dot{E}_{D,Sub} = \dot{E}_{20} + \dot{E}_{23} - \dot{E}_{21} - \dot{E}_{24}$
Turbine	$\dot{W}_{turb} = \dot{m}_{13}(h_{13}-h_{14})$	$\dot{E}_{D,turb} = \dot{E}_{13} - \dot{E}_{14} - \dot{W}_{turb}$	*Distillation column*	$\dot{m}_{18}h_{18} + \dot{m}_{40}h_{40} + \dot{m}_{32}h_{32} = \dot{m}_{41}h_{41} + \dot{m}_{19}h_{19} + \dot{m}_{25}h_{25}$	$\dot{E}_{D,DS} = \dot{E}_{18} + \dot{E}_{40} + \dot{E}_{32} - \dot{E}_{41} - \dot{E}_{19} - \dot{E}_{25} - \dot{E}_{33}$
Mixer	$\dot{m}_{24}h_{24} + \dot{m}_{27}h_{27} + \dot{m}_{15}h_{15} + \dot{m}_6 h_6 = \dot{m}_{16}h_{16}$	$\dot{E}_{D,mix} = \dot{E}_6 + \dot{E}_{15} + \dot{E}_{27} + \dot{E}_{24} - \dot{E}_{16}$	*Condenser*	$\dot{Q}_{Cond} = \dot{m}_{19}(h_{19}-h_{20}) = \dot{m}_{34}(h_{35}-h_{34})$	$\dot{E}_{D,Cond} = \dot{E}_{19} + \dot{E}_{34} - \dot{E}_{20} - \dot{E}_{35}$
Recuperator 1	$\dot{Q}_{Recup1} = \dot{m}_{14}(h_{14}-h_{15}) = \dot{m}_{2'}(h_{3'}-h_{2'})$	$\dot{E}_{D,Recup1} = \dot{E}_{2'} + \dot{E}_{14} - \dot{E}_{3'} - \dot{E}_{15}$	*Absorber 1*	$\dot{Q}_{Abs1} = \dot{m}_{16}(h_{16}-h_1) = \dot{m}_{29}(h_{29}-h_{28})$	$\dot{E}_{D,Abs1} = \dot{E}_{16} + \dot{E}_{28} - \dot{E}_1 - \dot{E}_{29}$
Recuperator 2	$\dot{Q}_{Recup2} = \dot{m}_{25}(h_{25}-h_{26}) = \dot{m}_{3'}(h_4-h_{3'})$	$\dot{E}_{D,Recup1} = \dot{E}_{3'} + \dot{E}_{25} - \dot{E}_4 - \dot{E}_{26}$	*Absorber 2*	$\dot{Q}_{Abs2} = \dot{m}_{7'}(h_{7'}-h_8) = \dot{m}_{30}(h_{31}-h_{30})$	$\dot{E}_{D,Abs2} = \dot{E}_{7'} + \dot{E}_{30} - \dot{E}_8 - \dot{E}_{31}$
Separator	$\dot{m}_4 h_4 = \dot{m}_{4'}h_{4'} + \dot{m}_{4''}h_{4''}$	$\dot{E}_{D,sep} = \dot{E}_4 - \dot{E}_{4'} - \dot{E}_{4''}$	*Evaporator*	$\dot{Q}_{Eva} = \dot{m}_{22}(h_{23}-h_{22}) = \dot{m}_{36}(h_{36}-h_{37})$	$\dot{E}_{D,Eva} = \dot{E}_{22} + \dot{E}_{36} - \dot{E}_{23} - \dot{E}_{37}$
Pre-heater 1	$\dot{Q}_{Pre1} = \dot{m}_9(h_{10}-h_9) = \dot{m}_{4'}(h_{4'}-h_5)$	$\dot{E}_{D,Pre1} = \dot{E}_{4'} + \dot{E}_9 - \dot{E}_5 - \dot{E}_{10}$	*HEX*	$\dot{Q}_{HEX} = \dot{m}_{41}(h_{41}-h_{42}) = \dot{m}_{46}(h_{43}-h_{46})$	$\dot{E}_{D,HEX} = \dot{E}_{41} + \dot{E}_{46} - \dot{E}_{43} - \dot{E}_{42}$
Pre-heater 2	$\dot{Q}_{Pre2} = \dot{m}_{4''}(h_{4''}-h_7) = \dot{m}_{17}(h_{18}-h_{17})$	$\dot{E}_{D,Pre1} = \dot{E}_{4''} + \dot{E}_{17} - \dot{E}_7 - \dot{E}_{18}$	*Compressor*	$\dot{W}_{Comp} = \dot{m}_{43}(h_{44}-h_{43})$	$\dot{E}_{D,Comp} = \dot{E}_{43} + \dot{W}_{Comp} - \dot{E}_{44}$
Pump 1	$\dot{W}_{pump1} = \dot{m}_1(h_2-h_1)$	$\dot{E}_{D,pump1} = \dot{W}_{pump1} + \dot{E}_1 - \dot{E}_2$	*Heater*	$\dot{Q}_{Heater} = \dot{m}_{44}(h_{44}-h_{45}) = \dot{m}_{47}(h_{48}-h_{47})$	$\dot{E}_{D,Heater} = \dot{E}_{44} + \dot{E}_{47} - \dot{E}_{45} - \dot{E}_{48}$
Pump 2	$\dot{W}_{pump2} = \dot{m}_{8'}(h_9-h_{8'})$	$\dot{E}_{D,pump2} = \dot{W}_{pump2} + \dot{E}_{8'} - \dot{E}_9$	*Throttle valve 6*	$\dot{m}_{45}h_{45} = \dot{m}_{46}h_{46}$	$\dot{E}_{D,Tv6} = \dot{E}_{45} - \dot{E}_{46}$
Pump 3	$\dot{W}_{pump3} = \dot{m}_{8''}(h_{17}-h_{8''})$	$\dot{E}_{D,pump3} = \dot{W}_{pump3} + \dot{E}_{8''} - \dot{E}_{17}$			

Table 3. Verification

Subsystem	*Parameter*	Value	
		Present study	[13]
Concentrated Solar Power	$\dot{Q}_{SUN}$ (kW)	64358	64358
	$\dot{Q}_{REC}$ (kW)	41369	41362
	$\dot{Q}_{REC,Loss}$ (kW)	10342	10344
	$\dot{Q}_{REC,NET}$ (kW)	31027	31025
Subsystem	***Parameter***	***Present study***	[14]
Kalina	Power (kW)	412	412.6
	Cooling (kW)	177	177
	Energy efficiency (%)	27.89	27.96
Subsystem	***Parameter***	***Present study***	[15]
Heat pump	Mass flow rate (kg/s)	200.7	201.6
	Compressor power(kW)	49384	49537
	COP	4.69	4.711

4.2. Energy and exergy analysis results

The analysis shows that the proposed system achieves 25.6% energy efficiency, 6.85% exergy efficiency, 3296 kW power output, 2500 kW cooling, and 14,300 kW heating capacity. As shown in Figure 2, the CSP subsystem contributes the largest share of exergy destruction at 69%.Figure 3 shows the exergy destruction in each component. Based on the results, the highest exergy destruction occurs in the heliostat field, receiver from the CSP subsystem, and HEX from heat pump, with values of 26,100 kW, 18,300 kW, and 4,600 kW, respectively. Figure 4 presents the exergy efficiency of each component. The throttle valves exhibit the highest exergy efficiency, exceeding 99%, while the lowest efficiencies are observed in Absorber 2, the heater, and the condenser, with values of 26.8%, 30%, and 45.6%, respectively.

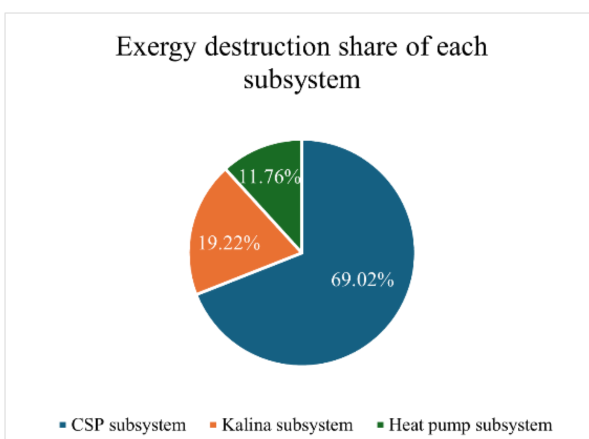

Figure 2. Exergy destruction share of each subsystem

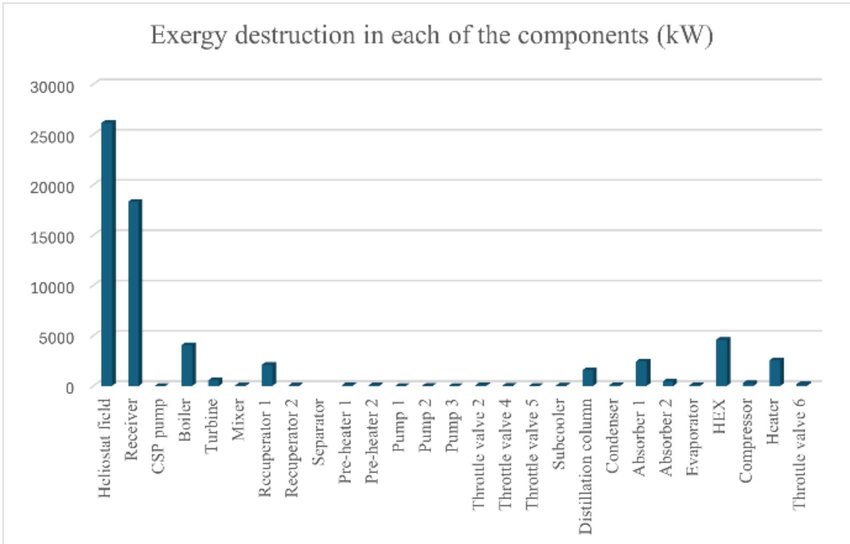

Figure 3. Exergy destruction share of each component (kW)

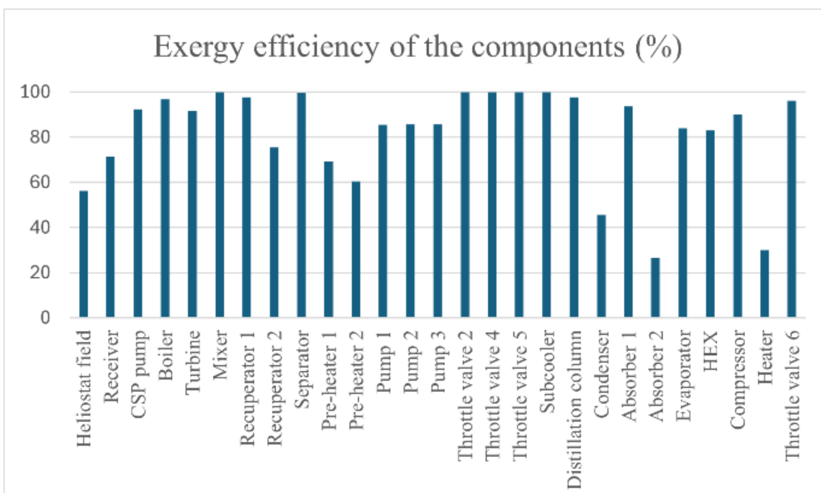

Figure 4. Exergy efficiency of each component (%)

4.3. Sensitivity

In the heliostat field, receiver from the CSP subsystem, and HEX from heat pump, with values of 26,100 kW, 18,300 kW, and 4,600 kW, respectively. Figure 4 presents the exergy efficiency of each component. The throttle valves exhibit the highest exergy efficiency, exceeding 99%, while the lowest efficiencies are observed in Absorber 2, the heater, and the condenser, with values of 26.8%, 30%, and 45.6%, respectively.

While the proposed system involves numerous variables, certain ones have a significantly greater influence on performance. To determine the most impactful parameters, a detailed analysis was conducted using Engineering Equation Solver (EES). The key variables identified are illustrated in the following figures. As shown in Figure 5, increasing DNI causes energy efficiency to decrease from 29.1% to 23.9%, while exergy efficiency increases from 5.3% to 7.6% over the same range. This occurs because higher DNI increases net work but significantly reduces heating load. While energy efficiency drops due to the energy balance, exergy efficiency rises since heat carries lower exergy value.

Figure 6 illustrates that increasing the turbine inlet temperature boosts turbine power output, but significantly reduces the cooling rate. As a result, energy efficiency decreases from 28.8% to 20.5%, while exergy efficiency rises from 6.1% to 8.2% over the range.

Figure 7 illustrates the impact of turbine isentropic efficiency on the system's energy and exergy efficiencies. As turbine efficiency increases, the turbine's power output rises, leading to a notable improvement in energy efficiency from 22% to 27.2%, and in exergy efficiency from 6.3% to 7.1% over the evaluated range.

Figure 8 shows the effect of compressor pressure ratio on system performance. As the pressure ratio increases, the required power also rises, while the heating load increases simultaneously. This results in minimal change in energy efficiency. However, exergy efficiency declines, since higher pressure ratios reduce net power output—and in exergy analysis, work carries more weight than heat.

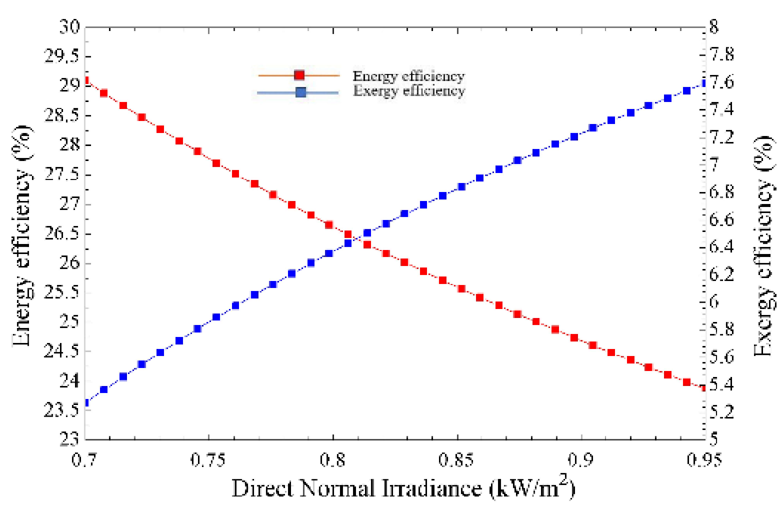

Figure 5. Impact of DNI on system performance

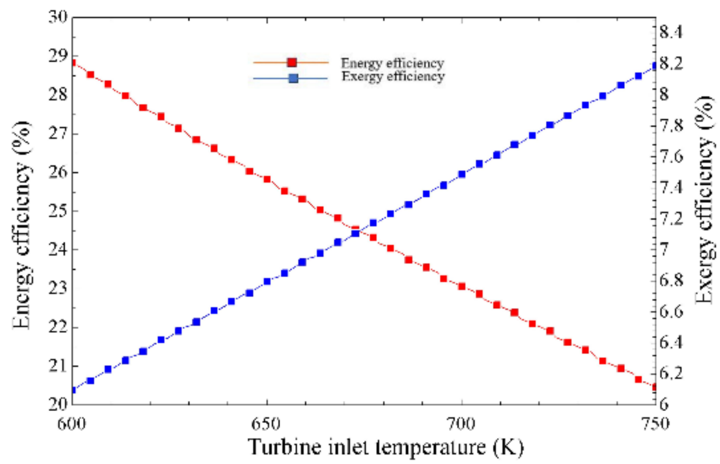

Figure 6. Effect of turbine inlet temperature on system performance

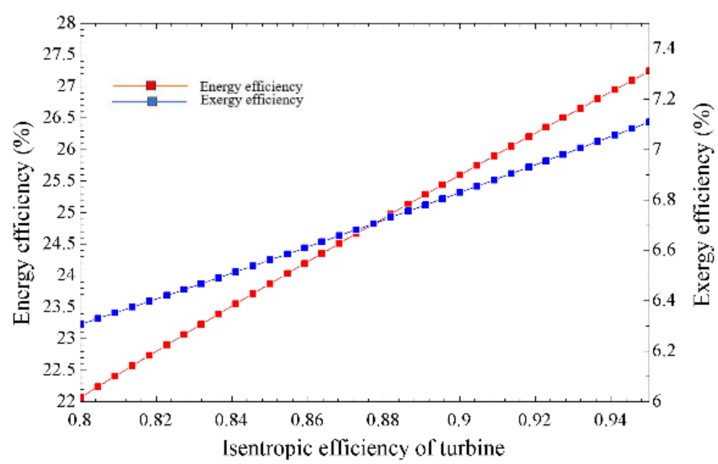

Figure 7. Impact of turbine isentropic efficiency on system performance

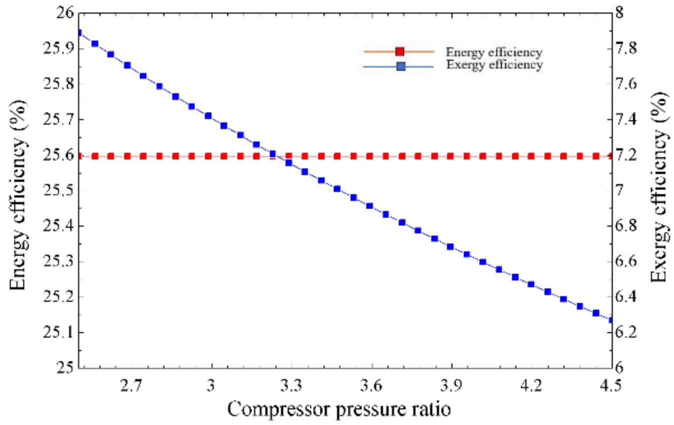

Figure 8. Impact of compressor pressure ratio on system performance

5. Conclusion

In conclusion, this study successfully designed and analyzed a novel, sustainable solar-based energy system integrating concentrated solar power (CSP), a modified Kalina cycle, and a heat pump to simultaneously produce electricity, cooling, and heating. The incorporation of thermal energy storage in the CSP subsystem enhances system reliability by addressing the intermittency typically associated with solar energy. The modified Kalina cycle used in this system is distinctive, featuring a distillation column that efficiently separates ammonia from the ammonia–water mixture to enable sub-zero cooling. Comprehensive energy and exergy analyses were conducted to evaluate system performance. Additionally, a sensitivity analysis was performed to assess the influence of four key parameters on overall system efficiency. The key findings of this study, outlined below, provide valuable insights into the design and optimization of advanced multi-generation energy systems:

- Energy analysis indicates that the proposed clean and sustainable system can generate 3,300 kW of power, 2,500 kW of cooling, and 14,300 kW of heating under baseline conditions, with an overall energy efficiency of 25.6%.
- Exergy analysis shows that the CSP subsystem accounts for the largest share of exergy destruction at 69%, followed by the Kalina cycle and heat pump at 19.2% and 11.8%, respectively. The overall exergy efficiency of the proposed system is 6.85%.
- Among all system components, the heliostat field contributes the most to exergy destruction, with 26,100 kW—over 40% of the total. The receiver and heat exchanger follow, accounting for 28.4% and 7.1%, respectively. Additionally, the throttle valves are

the most exergy-efficient components, while Absorber 2 and the heater are the least efficient, with exergy efficiencies of 26.8% and 30%, respectively.

- In the sensitivity analysis, four key parameters were identified as most impactful. The results show that increasing direct normal irradiance and turbine inlet temperature significantly reduces energy efficiency, while exergy efficiency rises sharply. Both energy and exergy efficiencies improve with higher turbine isentropic efficiency. However, increasing the compressor pressure ratio has little effect on energy efficiency, while it causes a slight decline in exergy efficiency.

Acknowledgment

The authors acknowledge the financial support provided by the European Union's Interreg Aurora (RESILIFY, Grant No. 20366468) and CETPartnership (OptiDCG4H2, Grant No. CETP-2023-00567, Enhance Europe CETP-2023-00061).

References

[1] W. Ma *et al.*, “Hydrogen generation system with zero carbon emission based on synergistic conversion of methane and solar energy,” *Energy*, vol. 316, p. 134609, 2025, doi: https://doi.org/10.1016/j.energy.2025.134609.

[2] A. Shokri Kalan, S. Heidarabadi, M. Khaleghi, H. Ghiasirad, and A. Skorek-Osikowska, “Biomass-to-energy integrated trigeneration system using supercritical CO2 and modified Kalina cycles: Energy and exergy analysis,” *Energy*, vol. 270, p. 126845, 2023, doi: https://doi.org/10.1016/j.energy.2023.126845.

[3] X. Huang *et al.*, “Thermodynamic analysis and optimization of a novel green hydrogen-electricity-heat tri-generation system based on full spectrum utilization of solar energy,” *Energy Convers Manag*, vol. 327, p. 119527, 2025, doi: https://doi.org/10.1016/j.enconman.2025.119527.

[4] D. S. Jayathunga, H. P. Karunathilake, M. Narayana, and S. Witharana, “Phase change material (PCM) candidates for latent heat thermal energy storage (LHTES) in concentrated solar power (CSP) based thermal applications - A review,” *Renewable and Sustainable Energy Reviews*, vol. 189, p. 113904, 2024, doi: https://doi.org/10.1016/j.rser.2023.113904.

[5] R. P. Merchán, M. J. Santos, A. Medina, and A. Calvo Hernández, “High temperature central tower plants for concentrated solar power: 2021 overview,” *Renewable and Sustainable Energy Reviews*, vol. 155, p. 111828, 2022, doi: https://doi.org/10.1016/j.rser.2021.111828.

[6] S. Noman Danish *et al.*, “Techno-economic analysis of the integration of an innovative particle-based concentrating solar power system with a thermally driven cooling system,” *Energy Convers Manag*, vol. 320, p. 118968, 2024, doi: https://doi.org/10.1016/j.enconman.2024.118968.

[7] M. A. Alharthi, A. Khaliq, S. Alqaed, and F. Almehmadi, “Investigation of new combined cooling, heating and power system based on solar thermal power and single-double-effect refrigeration cycle,” *Energy Reports*, vol. 9, pp. 289–309, 2023, doi: https://doi.org/10.1016/j.egyr.2023.04.002.

[8] M. Parvez, T. Ahamad, S. Lal, O. Khan, F. Khalid, and Z. Yahya, “Energy, Exergy, Economic, and environmental assessment of a trigeneration system for combined power, cooling, and water desalination system driven by solar energy,” *International Journal of Thermofluids*, vol. 22, p. 100694, 2024, doi: https://doi.org/10.1016/j.ijft.2024.100694.

[9] E. Enasel and G. Dumitrascu, “Storage solutions for renewable energy: A review,” *Energy Nexus*, vol. 17, p. 100391, 2025, doi: https://doi.org/10.1016/j.nexus.2025.100391.

[10] T. E. Boukelia, S. Djimli, A. Bourouis, Y. Kabar, and F. Hadjez, “Techno-economic analysis of integrated waste heat recovery, thermal storage, and backup systems for enhanced CSP dispatch capacity: A comparative study of different plant configurations,” *J Energy Storage*, vol. 118, p. 116231, 2025, doi: https://doi.org/10.1016/j.est.2025.116231.

[11] S. K. Singh, A. K. Das, and A. R. Dixit, “Performance of proton exchange membrane in solar-integrated Kalina cycle systems for green hydrogen production,” *Thermal Science and Engineering Progress*, vol. 60, p. 103413, 2025, doi: https://doi.org/10.1016/j.tsep.2025.103413.

[12] S. Rostami, H. Ghiasirad, H. Rostamzadeh, A. S. Kalan, and A. Maleki, “A wind turbine driven hybrid HDH-MED-MVC desalination system towards minimal liquid discharge,” *S Afr J Chem Eng*, vol. 44, pp. 356–369, 2023, doi: https://doi.org/10.1016/j.sajce.2023.03.007.

[13] V. Zare and M. Hasanzadeh, “Energy and exergy analysis of a closed Brayton cycle-based combined cycle for solar power tower plants,” *Energy Convers Manag*, vol. 128, pp. 227–237, 2016, doi: https://doi.org/10.1016/j.enconman.2016.09.080.

[14] A. S. Kalan, H. Ghiasirad, R. K. Saray, and S. Mirmasoumi, “Thermo-economic evaluation and multi-objective optimization of a waste heat driven combined cooling and power system based on a modified Kalina cycle,” *Energy Convers Manag*, vol. 247, p. 114723, 2021, doi: https://doi.org/10.1016/j.enconman.2021.114723.

[15] A. Pirmohamadi, H. Ghaebi, B. M. Ziapour, and M. Ebadollahi, “Exergoeconomic Analysis of a Novel Hybrid System by Integrating the Kalina and Heat Pump Cycles with a Nitrogen Closed Brayton System,” *Energy Reports*, vol. 7, pp. 546–564, 2021, doi: https://doi.org/10.1016/j.egyr.2021.01.009.

[16] R. Hajipour, E. Neshat, and A. S. Kalan, “Investigating the interactive effects of different functional parameters of a heating, cooling and power cycle based on DOE method,” *Case Studies in Thermal Engineering*, vol. 68, p. 105853, 2025, doi: https://doi.org/10.1016/j.csite.2025.105853.

[17] S. E. Trabelsi, R. Chargui, L. Qoaider, A. Liqreina, and A. Guizani, “Techno-economic performance of concentrating solar power plants under the climatic conditions of the southern region of Tunisia,” *Energy Convers Manag*, vol. 119, pp. 203–214, 2016, doi: https://doi.org/10.1016/j.enconman.2016.04.033.

[18] M. B. Khuyinrud, A. S. Kalan, H. Ghiasirad, T. Gholizadeh, X. Lü, and A. Arabkoohsar, “A novel biomass-to-energy cogeneration system using zeotropic mixtures: Multi-objective optimization and environmental assessment,” *Process Safety and Environmental Protection*, vol. 197, p. 106976, 2025, doi: https://doi.org/10.1016/j.psep.2025.106976.